

MuRF: Unlocking the Multi-Scale Potential of Vision Foundation Models

Bocheng Zou[†], Mu Cai[†], Mark Stanley^{*}, Dingfu Lu^{*}, and Yong Jae Lee¹

¹University of Wisconsin-Madison

Vision Foundation Models (VFMs) have become the cornerstone of modern computer vision, offering robust representations across a wide array of tasks. While recent advances allow these models to handle varying input sizes during training, inference typically remains restricted to a single, fixed scale. This prevalent single-scale paradigm overlooks a fundamental property of visual perception: varying resolutions offer complementary inductive biases, where low-resolution views excel at global semantic recognition and high-resolution views are essential for fine-grained refinement. In this work, we propose **Multi-Resolution Fusion (MuRF)**, a simple yet universally effective strategy to harness this synergy at inference time. Instead of relying on a single view, *MuRF* constructs a unified representation by processing an image at multiple resolutions through a frozen VFM and fusing the resulting features. The universality of *MuRF* is its most compelling attribute. It is not tied to a specific architecture, serving instead as a fundamental, training-free enhancement to visual representation. We empirically validate this by applying *MuRF* to a broad spectrum of critical computer vision tasks across multiple distinct VFM families—primarily DINOv2, but also demonstrating successful generalization to contrastive models like SigLIP2.

 **Date:** March 26, 2026

 **Projects:** <https://MuRF-VFM.github.io>

 **Code Repository:** <https://github.com/orgs/MuRF-VFM>

 **Contact:** bochengz@cs.wisc.edu

1. Introduction

The landscape of computer vision has been reshaped by standardizing visual representation learning through large-scale Vision Foundation Models (VFMs) (Oquab et al., 2024). These models, pre-trained on vast datasets, provide widely transferable features that serve as the bedrock for numerous downstream applications. A key axis of evolution in this domain has been handling image resolution. While early ViT-based approaches required rigid, fixed-size inputs (Dosovitskiy et al., 2021), recent paradigms like “multi resolution” training (e.g., DINOv2 (Oquab et al., 2024)) have enabled models to process images of arbitrary aspect ratios and scales flexibly.

Despite this flexibility in *training*, standard *inference* protocols remain surprisingly rigid. Typically, an input image is resized to a single “optimal” resolution before being processed by the VFM. We argue that this single-scale inference discards a wealth of information inherent in the multi-scale nature of visual data. As shown in Figure 1, it is well-understood that a “division of labor” exists across different viewing scales: low-resolution inputs, by virtue of their larger relative patch sizes, excel at capturing globally coherent semantic context (recognition). High-resolution inputs are indispensable for resolving fine-grained high-frequency details and precise boundaries (refinement). By restricting inference to any single scale, current methods inevitably compromise either global coherence or local precision.

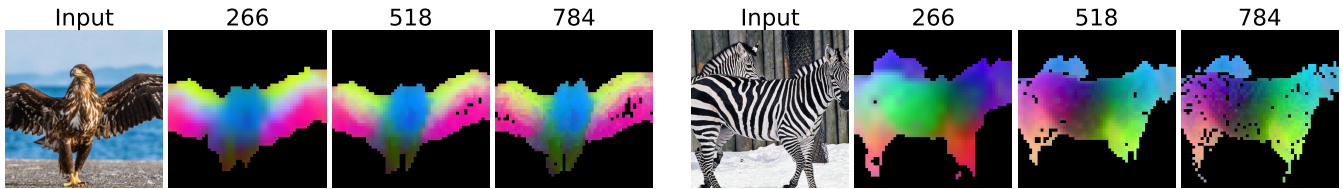


Figure 1: The “Recognition vs. Refinement” Dynamic. The feature map obtained when the input is resized to 266, 518, 784. At lower resolutions, the representation is globally coherent, enabling robust **recognition**. At higher resolutions, boundary details are sharper, enabling precise **refinement**, but the object’s interior becomes noisy, risking incomplete segmentation. Our work is motivated by synergizing these two roles.

We posit that unlocking the full potential of pre-trained VFMs requires actively aggregating these complementary views at inference time. To this end, we introduce **Multi-Resolution Fusion (*MuRF*)**, a general and straightforward strategy designed to create a scale-robust visual representation. Rather than modifying the VFM backbone, *MuRF* treats it as a frozen feature extractor. It processes the same input image across a pyramid of resolutions and fuses the resulting features into a unified representation. This simple operation effectively synergizes the recognition strengths of low-resolution views with the refinement capabilities of high-resolution views, without requiring expensive multi-scale training of the backbone itself.

The universality of *MuRF* is its most compelling attribute. It is not tied to a specific architecture or task but serves as a fundamental enhancement to the visual representation. We empirically validate this by applying *MuRF* to a broad spectrum of critical computer vision tasks, all using frozen VFM backbones:

- **Dense Prediction (Probing):** In semantic segmentation and depth estimation, simple linear heads trained on *MuRF* representations significantly outperform those trained on standard single-scale features, proving that multi-scale fusion enriches basic feature quality.
- **Multimodal Understanding:** When used as the visual encoder for Multimodal Large Language Models (MLLMs) in tasks like Visual Question Answering (VQA), *MuRF* provides LLMs with a more comprehensive visual context, enabling them to reason about both macroscopic scenes and microscopic details simultaneously.
- **Unsupervised Anomaly Detection:** In this training-free regime, *MuRF* effectively resolves the trade-off between detecting large structural anomalies and tiny surface defects, achieving state-of-the-art performance on demanding benchmarks like MVTEC AD 2 TEST_{priv,mix} (Heckler-Kram et al., 2025).

Our results suggest that effectively leveraging multi-resolution views at inference time is a general principle that consistently improves VFM-based systems. *MuRF* offers a simple, unified, and highly effective implementation of this principle.

2. Related Work

Our work explores unlocking the full potential of frozen VFMs by revisiting and modernizing multi-resolution inference strategies. We review the evolution of VFMs regarding standard input resolutions and discuss historical and contemporary approaches to multi-scale representation learning.

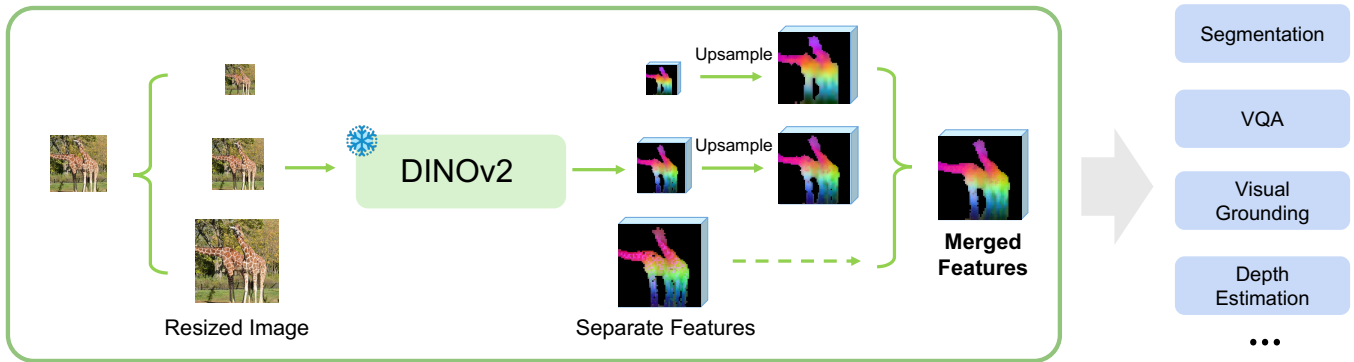


Figure 2: Overview of **Multi-Resolution Fusion (*MuRF*)**. An input image is resized to multiple resolutions and each view is processed by a frozen DINOv2 encoder to produce separate feature maps. These features are upsampled to a shared spatial resolution and fused into a single multi-resolution representation, which can then be used by lightweight task-specific heads for semantic segmentation, depth estimation, visual question answering, visual grounding, and other downstream tasks. Background is removed from the PCA figures.

2.1. Vision Foundation Models and Input Resolution

The field of computer vision has been fundamentally altered by the rise of Vision Foundation Models (VFMs). Initially dominated by Convolutional Neural Networks (CNNs) like ResNet (He et al., 2016) trained via supervised learning, the paradigm shifted toward Vision Transformers (ViTs) (Dosovitskiy et al., 2021) leveraging large-scale self-supervision. Models such as CLIP (Radford et al., 2021) and DINO/DINOv2 (Caron et al., 2021, Oquab et al., 2024) now serve as ubiquitous feature extractors across diverse tasks.

Traditionally, ViTs have been constrained by rigid input resolutions (e.g., 224×224) due to their reliance on fixed positional embeddings. This limitation often necessitates aggressive resizing or cropping, potentially discarding critical visual information. Recent advancements, such as DINOv2 (Oquab et al., 2024), NaViT (Dehghani et al., 2023) and FlexViT (Beyer et al., 2023), have introduced multi resolution or native resolution training, allowing models to process images in varying sizes during training.

While multi resolution *training* enhances model flexibility, standard *inference* protocols typically revert to utilizing a single, fixed scale, often the highest resolution practically affordable. This single-scale inference overlooks the inherent “division of labor” in visual perception: low-resolution views excel at global semantic recognition, while high-resolution views are necessary for fine-grained refinement. Our **Multi-Resolution Fusion (*MuRF*)** strategy addresses this by explicitly aggregating features from multiple resolutions at inference time, ensuring that both global context and local details are preserved without retraining the backbone.

2.2. Multi-Scale Representations

Handling objects of varying scales is a classical challenge in computer vision. Early approaches relied on *image pyramids* (Adelson et al., 1984), where an image is repeatedly resized and processed. While effective, this was computationally prohibitive for heavy older models. The deep learning era introduced *feature pyramids*, most notably Feature Pyramid Networks (FPN) (Lin et al., 2017), which efficiently construct multi-scale representations within the network’s forward pass.

In the era of frozen VFMs and Multimodal Large Language Models (MLLMs), explicitly constructing FPNs

often requires costly task-specific training. Consequently, recent trends have shifted back towards input-level manipulations. For handling high-resolution images in MLLMs (e.g., GPT-4V (OpenAI, 2023), LLaVA-NeXT (Liu et al., 2024b)), a common technique is dividing the image into smaller, fixed-resolution tiles (patches) processed independently, often supplemented by a single low-resolution global view. Similar tiling strategies have been applied in token efficiency for multimodal LLM, such as S^2 (Shi et al., 2025).

While tiling allows processing arbitrarily large images, it artificially breaks continuity, making it difficult for models to reason about objects that span splitting boundaries. Furthermore, simple upsampling techniques for VFM features, like FeatUp (Fu et al., 2024) and JAFAR (Couairon et al., 2025), may recover high-frequency details but do not inherently add new information absent from the original single-scale forward pass. What’s more, all of them require certain amount of training, which may lead to generalizability issues. *MuRF* revisits the classical image pyramid but modernizes it for the VFM era. By fusing multi-resolution views in the feature space, we avoid the boundary artifacts of tiling while capturing a richer, more holistic representation than single-scale upsampling, all in a completely training-free manner for the backbone.

3. Method

Our goal is to develop a universal, scale-robust visual representation from a frozen Vision Foundation Model (VFM) that can benefit a wide array of downstream tasks. To this end, we propose **Multi-Resolution Fusion (MuRF)**, a simple yet highly effective strategy for feature extraction at inference time. As illustrated in Figure 2, our method first constructs a rich, multi-scale feature map and then adapts this representation to specific tasks using lightweight, trainable heads.

3.1. Multi-Resolution Feature Fusion

The core of our approach is motivated by the observation that different input resolutions provide complementary visual information: low resolutions capture global context for robust **recognition**, while high resolutions provide fine-grained detail for precise **refinement**. *MuRF* explicitly harnesses this synergy by building a feature pyramid from the input space.

Given an input image $x \in \mathbb{R}^{H \times W \times C}$, we first create an input pyramid by resizing it to a set of different scaling factors, $S_{\text{res}} = \{s_1, s_2, \dots, s_k\}$. This yields a collection of images $\{x_s\}_{s \in S_{\text{res}}}$.

Each resized image x_s is then passed through a frozen VFM encoder, which we denote as Φ . We extract the feature map from the encoder (typically the last layer or a specific target block). For each resolution s , we obtain a patch-level feature map:

$$\mathcal{F}_s = \Phi(x_s) \in \mathbb{R}^{H_s \times W_s \times d} \quad (1)$$

where (H_s, W_s) are the spatial dimensions of the feature map for scale s , and d is the feature (channel) dimension.

To create a single, unified representation, we fuse these individual feature maps. Each map \mathcal{F}_s is first upsampled to a common target spatial resolution (H', W') , typically the original input size, using bilinear interpolation. These spatially-aligned feature maps are then concatenated along the channel dimension. This process yields the final **MuRF representation**, $\mathcal{F}_{\text{MuRF}}$:

$$\mathcal{F}_{\text{MuRF}} = \text{Concat}_{s \in S_{\text{res}}} (\text{Upsample}(\mathcal{F}_s)) \in \mathbb{R}^{H' \times W' \times D} \quad (2)$$

The total channel dimension D is the sum of the dimensions of the feature maps across all scales, $D = |S_{\text{res}}| \times d$.

This final tensor, \mathcal{F}_{MuRF} , serves as a powerful, frozen representation that is spatially rich, semantically deep, and robust to scale variations.

Why Channel-wise Concatenation? While one might consider alternative feature fusion operations—such as element-wise addition, mean pooling, or learnable attention—we intentionally select channel-wise concatenation. ViT features are highly localized and scale-dependent semantic tokens. Summation or mean pooling risks destructive interference, blending orthogonal scale-specific activations (e.g., a macroscopic semantic feature with a microscopic edge feature) into an ambiguous representation. By concatenating, we project the features into a higher-dimensional space ($D = |S_{res}| \times d$), preserving the strict independence of the “recognition” and “refinement” signals. This allows the lightweight downstream head to adaptively select and route the appropriate scale information without requiring a heavy, parameterized fusion network.

3.2. Task-Specific Adaptation

The \mathcal{F}_{MuRF} representation is task-agnostic. We adapt it to various downstream tasks by attaching lightweight, task-specific heads. This allows the frozen VFM backbone to be leveraged efficiently across different domains.

Dense Prediction Tasks. For tasks like semantic segmentation and depth estimation, which require a pixel-wise prediction, we attach a simple dense prediction head, $\text{Head}_{dense}(\cdot)$. This head typically consists of one or more convolutional layers (e.g., a 1×1 convolution) that project the D -dimensional feature channels to the desired number of output channels (e.g., number of semantic classes or a single depth value). The final prediction map $\hat{Y} \in \mathbb{R}^{H \times W \times C_{out}}$ is obtained by:

$$\hat{Y} = \text{Upsample}(\text{Head}_{dense}(\mathcal{F}_{MuRF})) \quad (3)$$

During training, only the parameters of Head_{dense} are updated, making the process highly efficient.

Unsupervised Anomaly Detection. This task follows a training-free paradigm. Instead of fusing features into a single tensor, we extend the nearest-neighbor approach. For each resolution s , we construct a dedicated memory bank \mathcal{M}_s from anomaly-free training images. At inference time, we compute a separate anomaly score map \hat{S}_s for each feature map \mathcal{F}_s by calculating the L_2 distance of each feature vector to its nearest neighbor in \mathcal{M}_s . The final, robust anomaly score map \hat{S} is produced by averaging all individual score maps after upsampling them to the original image dimensions:

$$\hat{S} = \frac{1}{|S_{res}|} \sum_{s \in S_{res}} \text{Upsample}(\hat{S}_s) \quad (4)$$

This fusion of scores leverages the strengths of all views for both recognition and refinement.

Multimodal Language Models. In the context of MLLMs for tasks like Visual Question Answering (VQA) and visual grounding, the \mathcal{F}_{DINOv2} representation serves as the visual input to the language model. The rich spatial feature map \mathcal{F}_{MuRF} is first passed through a perception module or projection layer, $\text{Head}_{MLLM}(\cdot)$, which maps the visual features into the word embedding space of the LLM.

$$E_{visual} = \text{Head}_{MLLM}(\mathcal{F}_{MuRF}) \quad (5)$$

These visual embeddings E_{visual} are then treated as a sequence of “visual tokens” and prepended to the text token embeddings. By providing the LLM with a representation that is rich in both global and local detail, we empower it to answer questions that require reasoning across multiple scales. Only the MLLM’s projection layer and other designated parameters are trained, while the *MuRF* feature extractor remains frozen.

4. Experiments

To validate the universality and effectiveness of our proposed **Multi-Resolution Fusion** (*MuRF*) representation, we conduct a comprehensive set of experiments across four diverse and fundamental computer vision tasks: semantic segmentation, depth estimation, visual question answering, and anomaly detection. Our evaluation aims to demonstrate that *MuRF* consistently improves performance over strong, single-scale baselines, regardless of the downstream application.

4.1. Experimental Setup

VFM Backbone and *MuRF* Configuration. Unless otherwise specified, our *MuRF* configuration is as follows:

- **Backbone:** Across all experiments, we use the publicly available, pre-trained **DINOv2-ViT-B/14** (Oquab et al., 2024) as our frozen VFM encoder. This ensures a fair comparison and highlights the gains attributable solely to our multi-resolution fusion strategy. We additionally experiment on **Siglip2-Base** (Patch16 NaFlex version) (Tschannen et al., 2025) to verify the applicability of our proposed approach.
- **Resolutions (S_{res}):** We are using 5 resolutions for anomaly detection, and 3 resolutions for the rest of tasks including segmentation, depth estimation, and PCA, and 2 resolutions for MLLM. We adhere to the resolution of the original implementation including LLaVA-1.5 (Liu et al., 2024a) and DINOv2 (Oquab et al., 2024).

The final *MuRF* representation is generated by upsampling all extracted feature maps to a common resolution and concatenating them channel-wise, as described in Section 3.1.

Training Details. For all downstream tasks (segmentation, depth estimation, and VQA), we exclusively train the task-specific heads while keeping both the VFM backbone and the *MuRF* fusion module frozen. We adhere to the optimization configurations—including optimizer, learning rate, and schedule—established in the respective original papers (Oquab et al., 2024, Liu et al., 2024b). Additional details of the experiment for reproducibility can be found in the Supplementary Material.

4.2. Semantic Segmentation

Setup. We evaluate on the challenging **ADE20k** (Zhou et al., 2019) and **PASCAL VOC** (Everingham et al., 2010) benchmark using the standard mean Intersection over Union (mIoU) metric. Our baseline for comparison is a linear probing setup using the same frozen DINOv2 encoder but with features extracted from a single input resolution, which represents the standard inference paradigm. All experiments are performed using DINOv2-ViT-B/14.

Results. Table 1 presents the main results. Our *MuRF*-based representation provides a significant performance boost over the strong single-scale baseline. Figure 3 qualitatively illustrates this improvement. This

Table 1: Combined downstream evaluation. **Semantic segmentation:** performance in mIoU (%) on ADE20K and PASCAL VOC (higher is better). **Depth estimation:** performance on NYU Depth V2 and SUN RGB-D reporting RMSE (lower is better). *MuRF* significantly outperforms single-scale baselines, highlighting the benefit of our multi-scale representation for dense prediction and geometric reasoning. **Bold** indicates the best performance, and underline indicates the second best. "Rel. Improv" measures the relative improvement over original DinoV2 (medium resolution)

Method	Arch.	Semantic Segmentation \uparrow		Depth Estimation \downarrow			
		ADE20K	PASCAL VOC	NYU Depth V2		SUN RGB-D	
				lin. 1	lin. 4	lin. 1	lin. 4
OpenCLIP (Cherti et al., 2023)	ViT-G/14	39.3	71.4	0.541	0.510	0.537	0.476
MAE (He et al., 2022)	ViT-H/14	33.3	67.6	0.517	0.483	0.545	0.523
DINO (Caron et al., 2021)	ViT-B/8	31.8	66.4	0.555	0.539	0.553	0.541
iBOT (Zhou et al., 2022)	ViT-L/16	44.6	<u>82.3</u>	0.417	0.387	<u>0.447</u>	<u>0.435</u>
Low Resolution	ViT-B/14	40.6	69.2	0.435	0.410	0.483	0.458
Medium Resolution	ViT-B/14	45.5	78.5	<u>0.394</u>	<u>0.372</u>	0.453	0.434
High Resolution	ViT-B/14	<u>46.1</u>	81.8	0.397	0.376	0.460	0.433
<i>MuRF</i> (Ours)	ViT-B/14	47.4	83.1	0.368	0.363	0.441	0.432
Rel. Improv	-	+4.2%	+5.9%	+6.6%	+2.4%	+2.6%	+0.5%

demonstrates that by combining global context from low resolutions and fine details from high resolutions, *MuRF* produces a feature map that is inherently better suited for dense prediction. For PASCAL VOC segmentation under the linear probing protocol, *MuRF* requires approximately 1.3 \times the training time of the single-resolution counterpart.

4.3. Depth Estimation

Setup. We test the in-domain learning capability on **NYU Depth V2** (Silberman et al., 2012) dataset and the transfer learning capability on **SUN RGB-D** dataset (Song et al., 2015). Following standard protocols, we report performance using Root Mean Squared Error (RMSE, lower is better). Our evaluation employs two linear probing configurations: **Lin. 1**, which utilizes features from the final transformer layer concatenated with the [CLS] token, and **Lin. 4**, which follows the same protocol but concatenates tokens from layers $l = \{3, 6, 9, 12\}$. For our *MuRF* method, these feature sets are extracted at multiple resolutions and fused. In both cases, we compare against a baseline frozen DINOv2 backbone with a single-scale input.

Table 2: Computational Cost and Efficiency Analysis on DINOv2-ViT-B/14. We compare the single-scale baselines against our multi-scale *MuRF* in terms of training latency, downstream head parameter count, and performance (RMSE on NYU Depth V2). *MuRF* achieves the best performance with a reasonable trade-off in computation.

Method	Resolution	Latency (ms/iter)	Head Params (M)	VRAM (GB)	RMSE \downarrow
Single-Scale	0.5 \times	11.36	0.39	0.36	0.435
Single-Scale	1.0 \times	22.61	0.39	0.43	0.394
Single-Scale	1.5 \times	32.55	0.39	0.54	0.397
<i>MuRF</i> (Ours)	{0.5, 1.0, 1.5}\times	58.35	1.18	0.56	0.368

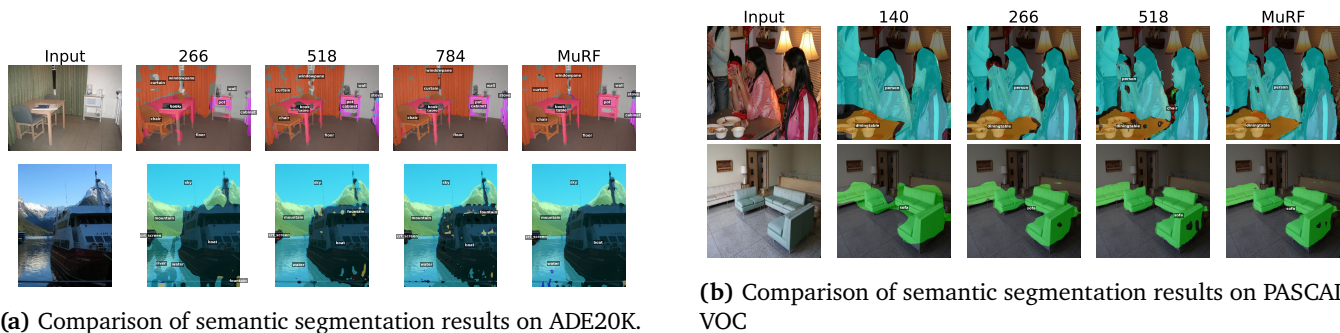


Figure 3: Qualitative comparison of semantic segmentation results on ADE20K (top) and PASCAL VOC (bottom) with different input resolutions. All images are resized to a square shape before being fed into DINOv2, and the subtitle above each image indicates the corresponding input resolution (side length in pixels).

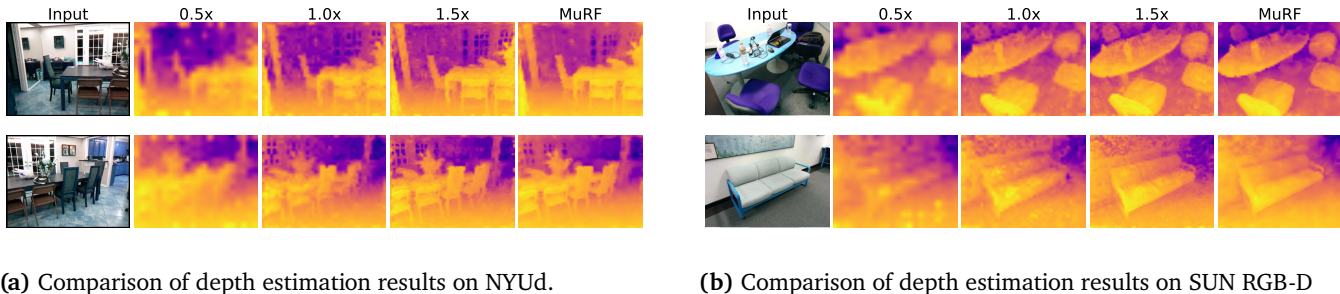


Figure 4: Qualitative depth estimation results on NYUd (left) and SUN RGB-D (right). We compare single-scale DINOv2 predictions at 0.5 \times , 1.0 \times , and 1.5 \times input resolutions with our *MuRF* fusion. By aggregating multi-resolution features, *MuRF* better preserves global scene structure while sharpening local geometry, producing smoother and more accurate depth maps. Labels 0.X \times indicate that the image fed into DINOv2 is resized to 0.X of the original image height and width.

Results. As shown in Table 1 and Figure 4, the model using our *MuRF* representation achieves substantially lower error rates. This indicates that the fusion of multi-scale features allows the prediction head to better reason about both the overall scene geometry (from low resolutions) and object boundaries (from high resolutions), leading to more accurate depth predictions. We have also measured the performance impact of *MuRF*, as demonstrated in Table 2.

4.4. Visual Question Answering

Setup. We integrate *MuRF* into an MLLM framework for VQA. The original vision encoder in LLaVA 1.5 is CLIP, which doesn’t have natural multi-resolution support. To verify how *MuRF* can support MLLMs, we apply *MuRF* on multiple variants of LLaVA 1.5, where we keep the same training recipe while changing the vision encoder.

In LLaVA’s DinoV2 variant, we use a single resolution input (336 \times 336) in DINOv2 as a baseline. For *MuRF*, we process resolutions of 224 and 336. In LLaVA’s SigLip2 variant, we use a single resolution input (384 \times 384) in SigLip2 as a baseline. For *MuRF*, we process resolutions of 256 and 384.

For all experiments, to prevent a computational bottleneck in the LLM, we must strictly avoid increasing the token sequence length (all experiments will have 576 visual tokens). Instead of appending multi-resolution

Table 3: LLaVA-MRF VQA Performance on MME(Fu et al., 2025), VLMsAreBiased (Bias)(Vo et al., 2026), V*(Wu and Xie, 2024), MME RealWord (MR)(Zhang et al., 2025b), RealWorld QA (RW)(xAI, 2024), GQA(Hudson and Manning, 2019), the total score obtained on four subset of mmbench (MMB)(Liu et al., 2025) ("cn_cc", "cn_dev", "en_dev", "ru_dev"), and the accuracy metric of POPE(Li et al., 2023). **Bold** indicates the best performance.

Vision Encoder	Res.	MME		Bias	V*	RW	MR	GQA	MMB	POPE
		Percept.	Cogn.							
CLIP (official LLaVA 1.5)	336	1511.4	347.1	16.2	50.3	56.1	26.5	62.0	195.4	86.9
DinoV2	336	1291.6	278.6	17.3	38.7	52.3	26.2	62.1	172.4	87.1
	224+336 (Ours)	1357.1	366.4	17.7	40.3	53.6	26.1	62.4	173.1	87.1
Clip+DinoV2	336	1403.4	243.9	15.8	48.7	53.6	31.5	62.2	194.2	86.4
	224+336 (Ours)	1471.2	281.4	16.3	48.2	56.7	31.8	62.9	198.8	87.4
SigLip2	384	1529.3	355.4	19.4	44.0	58.2	33.1	64.1	211.7	87.1
	256+384 (Ours)	1545.7	371.4	19.7	42.9	58.4	33.3	64.5	216.9	86.7

tokens sequentially, features from the low resolution (224 for DinoV2 and 256 for SigLip2) are spatially up-sampled and concatenated *patch-wise along the channel dimension* with the high resolution (336 for DinoV2 and 384 for SigLip2) features. The LLM’s visual projector then maps these high-channel-dimension tokens back to the standard LLM hidden dimension. **Crucially, this ensures the number of visual tokens fed into the LLM remains exactly the same as the single-resolution baseline**, incurring zero extra sequence-length computational cost for the LLM.

Results. The results in Table 3 show that equipping the MLLM with our *MuRF* representation strongly improves the multimodal understanding capacity regardless whether DinoV2 or SigLip2 is used as vision encoder. This suggests that the rich visual context provided by *MuRF* captures both holistic scene understanding and fine-grained details, empowers the language model to answer a wider range of visual questions more accurately. *MuRF* maintains comparable VRAM usage, as well as training and inference latency, relative to the single-resolution baseline. The Single-resolution baseline takes 71 minutes to pretrain, and 270 minutes to finetune, while *MuRF* takes 72 minutes to pretrain, and 274 minutes to finetune.

4.5. Unsupervised Anomaly Detection

Setup. Finally, we validate *MuRF* in a training-free setting on the **MVTec AD 2** (Heckler-Kram et al., 2025) benchmark, a challenging industrial inspection dataset. We use the pixel-level AU-PRO_{0.05} score as the primary metric and compare against state-of-the-art methods like PatchCore (Roth et al., 2022) and SuperAD (Zhang et al., 2025a).

For this experiment, we use a set of five scaling factors relative to the original image size: {0.3, 0.4, 0.5, 0.6, 0.7}.

Results. Table 4 confirms that our method achieves highly competitive, and in several cases state-of-the-art, performance. The ability of *MuRF* to handle anomalies of vastly different scales—from microscopic scratches to large, structural defects—is a direct result of its multi-resolution design, proving its effectiveness even without any parameter tuning.

Qualitatively, we sampled some results and presented them in Figure 5. The final “Merged” anomaly maps successfully combine the strengths of different input resolutions. Low-resolution views (e.g., 0.3×) are

Table 4: Anomaly detection performance (AU-PRO_{0.05} in %) on the MVTEC AD 2 dataset. *MuRF* demonstrates state-of-the-art results on TEST_{priv,mix} subset, showcasing its robustness in a challenging training-free scenario. "Training" means if the method involves parameter tuning within a neural network. **Bold** indicates the best performance, and underline indicates the second best.

Method	Training?	TEST _{priv}	TEST _{priv,mix}
PatchCore (Roth et al., 2022)	✗	62.3	52.6
SuperAD (Zhang et al., 2025a)	✗	61.2	59.3
RoBiS (Li et al., 2025)	✓	67.3	<u>59.7</u>
<i>MuRF</i> (Ours)	✗	<u>66.0</u>	62.3 ^{†+2.6}

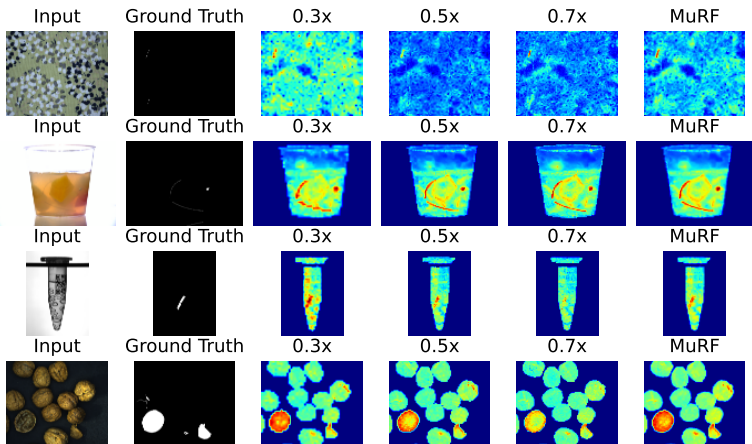


Figure 5: The visualization of anomaly detection on *MuRF* AD 2 TEST_{pub} dataset. Our merged result (*MuRF*) successfully combines the robust detection from low-resolution views (e.g., 0.3× correctly identifies the anomaly’s presence but with a coarse mask) and the sharp boundaries from high-resolution views (e.g., 0.7×).

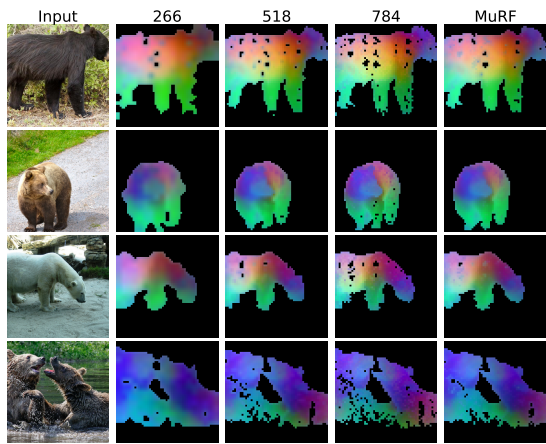


Figure 6: The PCA of feature embedding. It can be seen that lower resolution images tend to have better internal representation, but have worse boundaries due to low resolution. Higher resolution images tend to have sharper boundary but have holes in their internal. *MuRF* achieves a good balance that generates high-quality representation in both.

adept at robustly identifying the presence of an anomaly, though the resulting detection masks are coarse. Conversely, high-resolution views (e.g., 0.7×) provide sharp and precise boundaries for these anomalies. However, those views contain lots of noise or holes inside large anomaly areas (e.g., in walnuts). By fusing these different views, the *MuRF*-AD method produces more accurate and complete segmentation masks than single-resolution approaches like SuperAD (Zhang et al., 2025a).

4.6. Qualitative comparison

We present the PCA of DINOv2’s feature embedding on multiple resolutions, as well as our method’s feature embedding.

We have presented the results in Figure 6. It’s easy to see that high resolution images on the right provide sharper, more accurate boundaries. However, this focus on local detail comes at a cost: the model can lose global context, resulting in “holes” within the segmented region, while the low resolution images on the left’s internal is smoother. Our proposed approach *MuRF* (on the right) achieved a good balance.

4.7. Analysis of Resolution and Feature Concatenation

To show the benefits of *MuRF*, we conduct a controlled comparison against a standard feature concatenation baseline. To ensure a fair comparison over feature representation, we compare aggregating three distinct resolutions (*MuRF*) against aggregating three distinct encoder layers (Lin. 3).

The results, presented in Table 5, reveal a complementary relationship between multi-scale and multi-layer features. *MuRF* achieves superior performance on the in-domain NYU Depth V2 dataset (0.368 vs. 0.383), suggesting that scaling effectively captures the fine-grained structural details required for precise metric depth estimation. Conversely, the multi-layer approach (Lin. 3) generalizes better in the zero-shot setting on SUN RGB-D (0.437 vs. 0.441). This aligns with the intuition that intermediate Transformer layers retain robust, generic semantic abstractions.

Crucially, the best performance is achieved by combining both methodologies. This demonstrates that *MuRF* and multi-layer feature concatenations are not mutually exclusive; rather, they offer orthogonal benefits for complementary performance.

Table 5: Linear probing comparison for depth estimation reporting RMSE. We evaluate on NYU Depth V2 (in-domain) and SUN RGB-D (zero-shot). **Lin. 1** utilizes only the final layer. **Lin. 3** utilizes layers {4, 8, 12}. Lower scores indicate better performance. **Bold** indicates the best performance, underline indicates the second best.

Method	Resolutions	Layers	NYUd	SUN RGB-D
Lin. 1	1.0	12	0.394	0.453
<i>MuRF</i>	{0.5, 1.0, 1.5}	12	<u>0.368</u>	0.441
Lin. 3	0.5	{4, 8, 12}	0.415	0.462
Lin. 3	1.0	{4, 8, 12}	0.383	<u>0.437</u>
Lin. 3	1.5	{4, 8, 12}	0.387	0.446
Lin. 3 + <i>MuRF</i>	{0.5, 1.0, 1.5}	{4, 8, 12}	0.366	0.428

Table 6: Semantic segmentation performance in mIoU (%) when using SigLip2 as backbone. **Bold** indicates the best performance, underline indicates the second best.

Resolution	ADE20K↑
256	32.04
512	<u>35.27</u>
768	34.46
<i>MuRF</i> (Ours)	37.10 \uparrow +1.83

4.8. Ablation Study

We studied how the number of resolutions fused into *MuRF* has an impact on the performance on two downstream tasks: depth estimation and anomaly detection.

4.8.1. Depth Estimation

To isolate the contribution of each scale, we conduct an ablation study on the depth estimation task. We evaluate performance on NYUd using the **Lin. 1** protocol (reporting RMSE) while varying the specific resolutions used in our fusion. The results in Table 7 compare single-scale baselines against two-scale and our full three-scale *MuRF* method.

All three single-scale settings are clearly suboptimal compared to any multi-scale fusion: the best single-scale baseline (1.0 \times) achieves an RMSE of 0.394, whereas all two-scale variants already reduce the error to the 0.381–0.372 range, and the full *MuRF* configuration further improves it to 0.368. While the medium and high resolutions (1.0 \times and 1.5 \times) individually outperform the low-resolution setting (0.5 \times), including the coarsest view in the fusion remains beneficial. Comparing the best two-scale configuration (1.0 \times –1.5 \times ,

Table 7: *MuRF* ablation results for depth estimation. We compare single-scale baselines and two-scale fusions against the full three-scale *MuRF*. Performance is measured in RMSE (lower is better). The performance drops (indicated in red) are relative to the Full *MuRF* setting.

Setting	Resolutions			RMSE ↓
	0.5×	1.0×	1.5×	
<i>Single Resolution</i>				
1	✓			0.435 10.067
2		✓		0.394 10.026
3			✓	0.397 10.029
<i>Fused Resolutions</i>				
4	✓	✓		0.381 10.013
5	✓		✓	0.372 10.004
6		✓	✓	0.373 10.005
<i>MuRF</i>	✓	✓	✓	0.368

Table 8: Ablation study on Multi-Resolution Settings. Performance measured by AU-PRO_{0.05} on MV Tec AD 2 TEST_{pub} dataset is reported. We analyze the impact of different resolution combinations. The performance drops are relative to the Full *MuRF* setting.

Setting	Resolutions					AU-PRO _{0.05} ↑
	0.3×	0.4×	0.5×	0.6×	0.7×	
<i>Single Resolution</i>						
1	✓					52.29 15.03
2		✓				53.42 13.90
3			✓			55.39 11.93
4				✓		55.23 12.09
5					✓	54.87 12.45
<i>Fused Resolutions</i>						
6	✓		✓		✓	56.60 10.72
7	✓	✓		✓	✓	57.29 10.03
8			✓	✓	✓	57.05 10.27
<i>MuRF</i>	✓	✓	✓	✓	✓	57.32

RMSE 0.372) to full *MuRF* (0.5×–1.0×–1.5×, RMSE 0.368) shows that adding the low-resolution view still yields a measurable gain, even when two relatively strong scales are already present.

This pattern supports our hypothesis that low-resolution inputs provide complementary global geometric context that cannot be fully compensated by higher-resolution views alone. Overall, performance improves monotonically as we increase the number of fused resolutions, with diminishing but consistent returns, confirming that *MuRF*’s benefits stem from genuine multi-scale complementarity rather than from any single particularly “good” resolution.

4.8.2. Semantic Segmentation

We performed experiments on Siglip2-Base-Patch16-NaFlex (Tschannen et al., 2025) in addition to DINOv2-Base to verify the applicability of our proposed approach. Since SigLIP2 uses patch size of 16 instead of 14, we used the following combination of resolutions: $S_{\text{res}} = \{256, 512, 768\}$. Results are presented in Table 6.

4.8.3. Anomaly Detection

We evaluated different combinations of resolutions to test how the number of resolutions and how the choice of different resolutions have an impact on performance. We used AU-PRO_{0.05} on the MV Tec AD 2 TEST_{pub} dataset to evaluate the performance.

As with depth estimation, single-scale models are consistently weaker than their multi-scale counterparts, shown in Table 8. The best single resolution is 0.5× (55.39 AU-PRO_{0.05}), while both lower (0.3×, 52.29) and higher (0.7×, 54.87) scales alone underperform, indicating that extremely coarse views lose too much detail and extremely fine views become overly sensitive to local noise. Fusing multiple nearby resolutions mitigates these issues: a three-scale fusion of {0.3, 0.5, 0.7} already improves performance to 56.60, and adding additional intermediate scales ({0.3, 0.4, 0.6, 0.7}) further raises it to 57.29, nearly matching the full

five-scale *MuRF* (57.32). Notably, different multi-scale subsets with overlapping ranges (e.g., $\{0.5, 0.6, 0.7\}$) perform similarly well, suggesting that what matters most is covering a spectrum of coarse-to-fine views rather than any particular “magic” resolution.

These trends align with our qualitative findings in Fig. 5: coarse resolutions excel at reliably localizing anomalous regions but yield coarse masks, while finer resolutions sharpen boundaries but may miss parts of large defects. The progressive improvement from single- to multi-resolution settings confirms that *MuRF*’s anomaly detection gains arise from combining these complementary behaviors across scales, rather than from a specific hand-picked input size.

5. Conclusion

In this work, we introduced **Multi-Resolution Fusion** (*MuRF*), a simple yet powerful inference-time strategy to enhance Vision Foundation Models representations. By constructing a feature pyramid from the input space and fusing the resulting representations, *MuRF* effectively synergizes the global context from low-resolution views with the fine-grained detail from high-resolution ones. Our extensive experiments demonstrate that this single, unified approach yields consistent and significant performance gains across a diverse set of fundamental vision tasks, including dense prediction, multimodal reasoning, and unsupervised anomaly detection. These results establish multi-resolution aggregation not as a task-specific trick, but as a general principle for unlocking the full potential of pre-trained visual encoders.

6. Acknowledgment

This work was supported in part by NSF IIS2404180 and the Institute of Information & Communications Technology Planning & Evaluation (IITP) grants funded by the Korea government (MSIT) (No.RS-2025-02219317, AI Star Fellowship (Kookmin University)), (No. 2022-0-00871, Development of AI Autonomy and Knowledge Enhancement for AI Agent Collaboration), (No. RS-2022-00187238, Development of Large Korean Language Model Technology for Efficient Pretraining), and (No. RS-2025-2543949. Environment-Aware and Domain-Adaptive Multimodal Embodied AI for Real-World Interaction).

References

- Edward H Adelson, Charles H Anderson, James R Bergen, Peter J Burt, and Joan M Ogden. Pyramid methods in image processing. *RCA engineer*, 29(6):33–41, 1984.
- Lucas Beyer, Pavel Izmailov, Alexander Kolesnikov, Mathilde Caron, Simon Kornblith, Xiaohua Zhai, Matthias Minderer, Michael Tschannen, Ibrahim Alabdulmohsin, and Filip Pavetic. Flexivit: One model for all patch sizes. In *Proceedings of the IEEE/CVF Conference on Computer Vision and Pattern Recognition (CVPR)*, pages 14496–14506, June 2023.
- Mathilde Caron, Hugo Touvron, Ishan Misra, Hervé Jégou, Julien Mairal, Piotr Bojanowski, and Armand Joulin. Emerging properties in self-supervised vision transformers. In *Proceedings of the IEEE/CVF International Conference on Computer Vision (ICCV)*, pages 9650–9660, October 2021.
- Mehdi Cherti, Romain Beaumont, Ross Wightman, Mitchell Wortsman, Gabriel Ilharco, Cade Gordon, Christoph Schuhmann, Ludwig Schmidt, and Jenia Jitsev. Reproducible scaling laws for contrastive language-image learning. In *Proceedings of the IEEE/CVF Conference on Computer Vision and Pattern Recognition (CVPR)*, pages 2818–2829, June 2023.
- Paul Couairon, Loick Chambon, Louis Serrano, Jean-Emmanuel Haugeard, Matthieu Cord, and Nicolas Thome. Jafar: Jack up any feature at any resolution. *arXiv preprint arXiv:2506.11136*, 2025.
- Mostafa Dehghani, Basil Mustafa, Josip Djolonga, Jonathan Heek, Matthias Minderer, Mathilde Caron, Andreas Steiner, Joan Puigcerver, Robert Geirhos, Ibrahim M Alabdulmohsin, Avital Oliver, Piotr Padlewski, Alexey Gritsenko, Mario Lucic, and Neil Houlsby. Patch n’ pack: Navit, a vision transformer for any aspect ratio and resolution. In A. Oh, T. Naumann, A. Globerson, K. Saenko, M. Hardt, and S. Levine, editors, *Advances in Neural Information Processing Systems*, volume 36, pages 2252–2274. Curran Associates, Inc., 2023. URL https://proceedings.neurips.cc/paper_files/paper/2023/file/06ea400b9b7cfce6428ec27a371632eb-Paper-Conference.pdf.
- Alexey Dosovitskiy, Lucas Beyer, Alexander Kolesnikov, Dirk Weissenborn, Xiaohua Zhai, Thomas Unterthiner, Mostafa Dehghani, Matthias Minderer, Georg Heigold, Sylvain Gelly, Jakob Uszkoreit, and Neil Houlsby. An image is worth 16x16 words: Transformers for image recognition at scale. In *International Conference on Learning Representations*, 2021. URL <https://openreview.net/forum?id=YicbFdNTTy>.
- Mark Everingham, Luc Gool, Christopher K. Williams, John Winn, and Andrew Zisserman. The pascal visual object classes (voc) challenge. *Int. J. Comput. Vision*, 88(2):303–338, June 2010. ISSN 0920-5691. doi: 10.1007/s11263-009-0275-4. URL <https://doi.org/10.1007/s11263-009-0275-4>.
- Chaoyou Fu, Peixian Chen, Yunhang Shen, Yulei Qin, Mengdan Zhang, Xu Lin, Jinrui Yang, Xiawu Zheng, Ke Li, Xing Sun, Yunsheng Wu, Rongrong Ji, Caifeng Shan, and Ran He. MME: A comprehensive evaluation benchmark for multimodal large language models. In *The Thirty-ninth Annual Conference on Neural Information Processing Systems Datasets and Benchmarks Track*, 2025. URL <https://openreview.net/forum?id=DgH9YCsqWm>.
- Stephanie Fu, Mark Hamilton, Laura E. Brandt, Axel Feldmann, Zhoutong Zhang, and William T. Freeman. Featup: A model-agnostic framework for features at any resolution. In *The Twelfth International Conference on Learning Representations*, 2024. URL <https://openreview.net/forum?id=GkJiNn2QDF>.
- Kaiming He, Xiangyu Zhang, Shaoqing Ren, and Jian Sun. Deep residual learning for image recognition. In *Proceedings of the IEEE Conference on Computer Vision and Pattern Recognition (CVPR)*, June 2016.

- Kaiming He, Xinlei Chen, Saining Xie, Yanghao Li, Piotr Dollár, and Ross Girshick. Masked autoencoders are scalable vision learners. In *Proceedings of the IEEE/CVF Conference on Computer Vision and Pattern Recognition (CVPR)*, pages 16000–16009, June 2022.
- Lars Heckler-Kram, Jan-Hendrik Neudeck, Ulla Scheler, Rebecca König, and Carsten Steger. The mvtec ad 2 dataset: Advanced scenarios for unsupervised anomaly detection. *arXiv preprint arXiv:2503.21622*, 2025.
- Drew A. Hudson and Christopher D. Manning. Gqa: A new dataset for real-world visual reasoning and compositional question answering. In *Proceedings of the IEEE/CVF Conference on Computer Vision and Pattern Recognition (CVPR)*, June 2019.
- Xurui Li, Zhonsheng Jiang, Tingxuan Ai, and Yu Zhou. Robis: Robust binary segmentation for high-resolution industrial images. *arXiv preprint arXiv:2505.21152*, 2025.
- Yifan Li, Yifan Du, Kun Zhou, Jinpeng Wang, Xin Zhao, and Ji-Rong Wen. Evaluating object hallucination in large vision-language models. In Houda Bouamor, Juan Pino, and Kalika Bali, editors, *Proceedings of the 2023 Conference on Empirical Methods in Natural Language Processing*, pages 292–305, Singapore, December 2023. Association for Computational Linguistics. doi: 10.18653/v1/2023.emnlp-main.20. URL <https://aclanthology.org/2023.emnlp-main.20/>.
- Tsung-Yi Lin, Piotr Dollár, Ross Girshick, Kaiming He, Bharath Hariharan, and Serge Belongie. Feature pyramid networks for object detection. In *Proceedings of the IEEE conference on computer vision and pattern recognition*, pages 2117–2125, 2017.
- Haotian Liu, Chunyuan Li, Yuheng Li, and Yong Jae Lee. Improved baselines with visual instruction tuning. In *Proceedings of the IEEE/CVF Conference on Computer Vision and Pattern Recognition*, pages 26296–26306, 2024a.
- Haotian Liu, Chunyuan Li, Yuheng Li, Bo Li, Yuanhan Zhang, Sheng Shen, and Yong Jae Lee. Llava-next: Improved reasoning, ocr, and world knowledge, January 2024b. URL <https://llava-vl.github.io/blog/2024-01-30-llava-next/>.
- Yuan Liu, Haodong Duan, Yuanhan Zhang, Bo Li, Songyang Zhang, Wangbo Zhao, Yike Yuan, Jiaqi Wang, Conghui He, Ziwei Liu, Kai Chen, and Dahua Lin. Mmbench: Is your multi-modal model an all-around player? In Aleš Leonardis, Elisa Ricci, Stefan Roth, Olga Russakovsky, Torsten Sattler, and Gül Varol, editors, *Computer Vision – ECCV 2024*, pages 216–233, Cham, 2025. Springer Nature Switzerland. ISBN 978-3-031-72658-3.
- OpenAI. Gpt-4v(ision) system card, 2023.
- Maxime Oquab, Timothée Darcet, Théo Moutakanni, Huy V. Vo, Marc Szafraniec, Vasil Khalidov, Pierre Fernandez, Daniel HAZIZA, Francisco Massa, Alaaeldin El-Nouby, Mido Assran, Nicolas Ballas, Wojciech Galuba, Russell Howes, Po-Yao Huang, Shang-Wen Li, Ishan Misra, Michael Rabbat, Vasu Sharma, Gabriel Synnaeve, Hu Xu, Herve Jegou, Julien Mairal, Patrick Labatut, Armand Joulin, and Piotr Bojanowski. DINOv2: Learning robust visual features without supervision. *Transactions on Machine Learning Research*, 2024. ISSN 2835-8856. URL <https://openreview.net/forum?id=a68SUt6zFt>. Featured Certification.
- Alec Radford, Jong Wook Kim, Chris Hallacy, Aditya Ramesh, Gabriel Goh, Sandhini Agarwal, Girish Sastry, Amanda Askell, Pamela Mishkin, Jack Clark, Gretchen Krueger, and Ilya Sutskever. Learning transferable visual models from natural language supervision. In Marina Meila and Tong Zhang, editors, *Proceedings of*

- the 38th International Conference on Machine Learning*, volume 139 of *Proceedings of Machine Learning Research*, pages 8748–8763. PMLR, 18–24 Jul 2021. URL <https://proceedings.mlr.press/v139/radford21a.html>.
- Karsten Roth, Latha Pemula, Joaquin Zepeda, Bernhard Schölkopf, Thomas Brox, and Peter Gehler. Towards total recall in industrial anomaly detection. In *Proceedings of the IEEE/CVF conference on computer vision and pattern recognition*, pages 14318–14328, 2022.
- Baifeng Shi, Ziyang Wu, Maolin Mao, Xin Wang, and Trevor Darrell. When do we not need larger vision models? In Aleš Leonardis, Elisa Ricci, Stefan Roth, Olga Russakovsky, Torsten Sattler, and Gül Varol, editors, *Computer Vision – ECCV 2024*, pages 444–462, Cham, 2025. Springer Nature Switzerland. ISBN 978-3-031-73242-3.
- Nathan Silberman, Derek Hoiem, Pushmeet Kohli, and Rob Fergus. Indoor segmentation and support inference from rgb-d images. In Andrew Fitzgibbon, Svetlana Lazebnik, Pietro Perona, Yoichi Sato, and Cordelia Schmid, editors, *Computer Vision – ECCV 2012*, pages 746–760, Berlin, Heidelberg, 2012. Springer Berlin Heidelberg. ISBN 978-3-642-33715-4.
- Shuran Song, Samuel P. Lichtenberg, and Jianxiong Xiao. Sun rgb-d: A rgb-d scene understanding benchmark suite. In *2015 IEEE Conference on Computer Vision and Pattern Recognition (CVPR)*, pages 567–576, 2015. doi: 10.1109/CVPR.2015.7298655.
- Michael Tschannen, Alexey Gritsenko, Xiao Wang, Muhammad Ferjad Naeem, Ibrahim Alabdulmohsin, Nikhil Parthasarathy, Talfan Evans, Lucas Beyer, Ye Xia, Basil Mustafa, et al. Siglip 2: Multilingual vision-language encoders with improved semantic understanding, localization, and dense features. *arXiv preprint arXiv:2502.14786*, 2025.
- An Vo, Khai-Nguyen Nguyen, Mohammad Reza Taesiri, Vy Tuong Dang, Anh Totti Nguyen, and Daeyoung Kim. Vision language models are biased. In *The Fourteenth International Conference on Learning Representations*, 2026. URL <https://openreview.net/forum?id=DG4S201GQA>.
- Penghao Wu and Saining Xie. V?: Guided visual search as a core mechanism in multimodal llms. In *Proceedings of the IEEE/CVF Conference on Computer Vision and Pattern Recognition (CVPR)*, pages 13084–13094, June 2024.
- xAI. Grok-1.5, 2024.
- Huaiyuan Zhang, Hang Chen, Yu Cheng, Shunyi Wu, Linghao Sun, Linao Han, Zeyu Shi, and Lei Qi. Superad: A training-free anomaly classification and segmentation method for cvpr 2025 vand 3.0 workshop challenge track 1: Adapt & detect. *arXiv preprint arXiv:2505.19750*, 2025a.
- YiFan Zhang, Huanyu Zhang, Haochen Tian, Chaoyou Fu, Shuangqing Zhang, Junfei Wu, Feng Li, Kun Wang, Qingsong Wen, Zhang Zhang, Liang Wang, and Rong Jin. MME-realworld: Could your multimodal LLM challenge high-resolution real-world scenarios that are difficult for humans? In *The Thirteenth International Conference on Learning Representations*, 2025b. URL <https://openreview.net/forum?id=k5VHHgsRbi>.
- Bolei Zhou, Hang Zhao, Xavier Puig, Tete Xiao, Sanja Fidler, Adela Barriuso, and Antonio Torralba. Semantic understanding of scenes through the ade20k dataset. *International Journal of Computer Vision*, 127(3): 302–321, 2019.

Jinghao Zhou, Chen Wei, Huiyu Wang, Wei Shen, Cihang Xie, Alan Yuille, and Tao Kong. Image BERT pre-training with online tokenizer. In *International Conference on Learning Representations*, 2022. URL <https://openreview.net/forum?id=ydopy-e6Dg>.